Ground-plane-less bidirectional terahertz absorber based on omega resonators

Alexei Balmakou,[1,2,*] Maxim Podalov,[2] Sergei Khakhomov,[2] Doekele Stavenga,[1] and Igor Semchenko[2]

[1]*Department of Computational Physics, Zernike Institute for Advanced Materials, University of Groningen, 9747AG Groningen, The Netherlands*

[2]*Department of Physics, Gomel State University, 246019 Gomel, Belarus*

**Corresponding author: a.balmakou@rug.nl*

Received March 12, 2015; revised April 2, 2015; accepted April 11, 2015; posted April 13, 2015 (Doc. ID 236100); published April 30, 2015

We present a new ultrathin metamaterial that acts as a frequency-selective absorber of terahertz radiation. The absorber is a square array of pairs of omega-shaped micro-resonators made of high-ohmic-loss metal. The metamaterial provides significant suppression of transmitted and reflected radiation in a bidirectional regime (that is, for both forward and backward propagating radiation). The absorber is efficient in a wide range of angles of incidence. The absence of a ground plane makes the absorber unique in comparison with numerous analogs with a ground plane that operate in a unidirectional regime. The novel metamaterial potentially enables controllable transmission of terahertz radiation in imaging systems. Analytical calculations as well as finite-element electromagnetic modeling are presented for an exemplary case with peak absorption at ~3 THz.

OCIS codes: (350.2450) Filters, absorption; (160.3918) Metamaterials; (110.6795) Terahertz imaging.
http://dx.doi.org/10.1364/OL.40.002084

The development of frequency selective and wideband absorbers in the gigahertz [1], terahertz (THz) [2–4], infrared [5,6], and visible frequency ranges [7,8] is rapidly progressing. These devices are necessary elements for controlling the optical transmission and reflection in THz imaging and information-encoding systems. They have great potential for applications in astronomy, biology, medicine, security inspection, spectroscopy, telecommunications, and data transfer. The overwhelming majority of the existing optical absorbers have a metal ground plane, which acts as an almost perfect reflector and thus blocks transmission. Consequently, these devices can only operate in a unidirectional regime and thus are not suitable for THz imaging. The first symmetrical perfect absorber of gigahertz radiation is, to the best of our knowledge, the metamaterial consisting of helices presented in [9]. Very recently, experimental verification and theoretical explanations of a near-perfect absorber with compensated chirality have been reported [10]. However, that design is impractical for the THz frequency range, because (1) the required small thickness of the helices (radius $\sim 10^{-3}$ wavelength) causes fabrication difficulties, (2) in THz imaging it is extremely difficult to make the unit cell (a pixel) switchable from the transparent to the opaque regime, and (3) its large unit cell size is comparable with the wavelength, which limits the spatial resolution and thus the imaging quality.

Here we present a design of a near-perfect absorber of THz radiation without a ground plane, consisting of an array of so-called omega particles [11]. The array is a square lattice, where each unit cell is composed of four pairs of orthogonally arranged omega particles (Fig. 1). We applied analytical calculations and finite element modeling to find the optimal geometry of the omegas, array periodicity and material parameters that create a matched impedance of the array to that of free space and a strong electromagnetic response in every unit cell of the array, so obtaining a strongly reduced reflectance as well as destructive interference of the transmitted waves.

We previously developed an analytical model of omega particles [12], where we derived that incident radiation causes resonance with a strong harmonic electric current (indicated in Fig. 2) when the geometrical parameters of the omega particles satisfy the condition of equality of electric, magnetic, and magneto-electric polarizabilities. The local electric dipole moment (or electric response) $\mathbf{p} = -\int_{(V)} e\eta \mathbf{S}(l)\mathrm{d}V$ and magnetic dipole moment $\mathbf{m} = \frac{1}{2}\int_{(V)}(\mathbf{r}\times\mathbf{j})\mathrm{d}V$ are connected by the condition $|\mathbf{p}| = |\mathbf{m}|/c$; here $-e$ is the electron charge, η is the volume density of electrons, $\mathbf{S}(l)$ is the electron displacement vector at location l, $dV = S_{\perp}dl$ is the volume of an omega segment, with dl the length and $S_{\perp} = \pi d^2/4$ the cross-section of the segment (d is the diameter of the wire), $\mathbf{r}$ is the radius-vector of the particle, $\mathbf{j}$ is the current

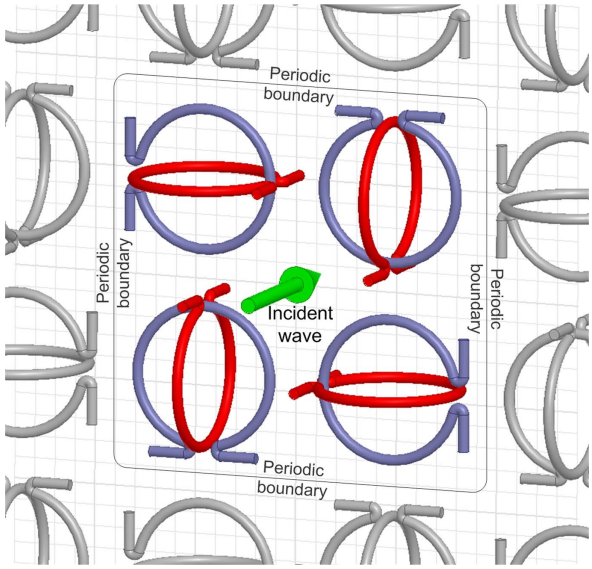

Fig. 1. Schematic of the array of pairs of omega particles. The unit cell is marked by the periodic boundary line. The green arrow indicates normally incident radiation.

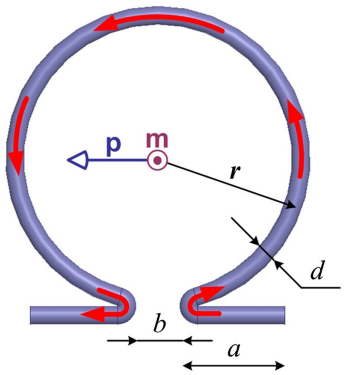

Fig. 2. Geometrical parameters of an omega particle (see text). The red arrows indicate the local electric current.

density vector, and c is the speed of light. **p** and **m** are tuned by the shape of the omega particle and, in turn, create scattered electromagnetic radiation [11,13–15].

For an omega particle with length L, the resonance wavelength is $\lambda_{\mathrm{res}} \approx 2L$. To achieve maximal absorption of radiation at the resonance wavelength, the radius of the loop has to be $r = \lambda_{\mathrm{res}}(\sqrt{2}-1)/2\pi$ [12]. As an example, we have assumed a resonance wavelength of $\lambda_{\mathrm{res}} = 100$ μm (3 THz), so that the required geometric parameter values of the omega particles become $L \approx 50$ μm and $r = 6.6$ μm, or, assuming a wire diameter $d = 1$ μm and gap width $b \approx 1.5$ μm, it follows with $a = (L - 2\pi r + b)/2$ that $a \approx 5$ μm (Fig. 2). Using these values in the finite-element method solver Ansys HFSS, we have calculated the reflectance R, transmittance T, and absorptance $A = 1 - R - T$, as a function of radiation frequency for various values of the lattice parameter. This yielded 37 μm as the optimal value of the lattice parameter, which we used in further calculations. With $2r = 13.2$ μm $\approx \lambda_{\mathrm{res}}/7$, the array can be called ultrathin.

Figure 3 diagrammatically shows the array with normally and obliquely incident light, which can be TE- or TM-polarized.

Figure 4 shows the frequency dependence of the transmittance, reflectance, and absorptance for normally incident radiation ($\alpha = 0°$). The resonance frequency was found to be 2.9 THz, slightly lower than the aimed for 3.0 THz, but the latter value could be easily realized with adjusted geometrical values of the omega particles.

Because of the four-fold array symmetry, the spectra for TE- and TM-waves are identical at normal incidence $\alpha = 0°$, but this is no longer the case for angles of incidence $\alpha > 0°$. Figure 5 presents the transmittance, reflectance, and absorptance spectra for angles of incidence

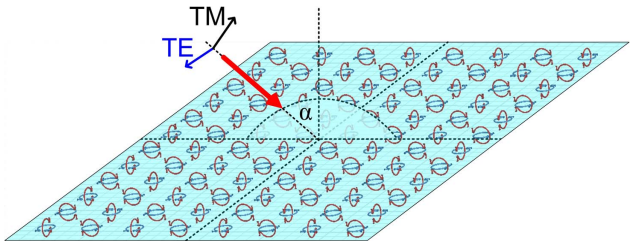

Fig. 3. Diagram of the omega particle array and incident TE- and TM-polarized radiation with angle of incidence α.

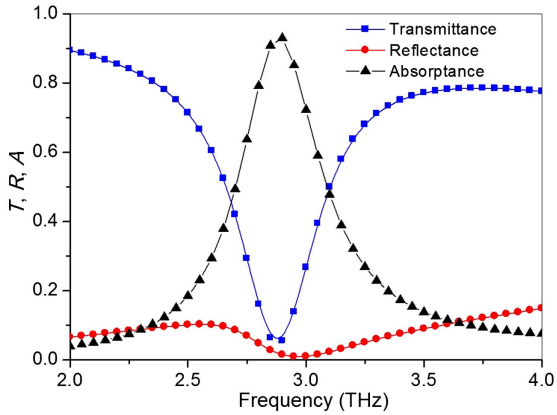

Fig. 4. Transmittance (T), reflectance (R), and absorptance (A) versus frequency at normal incidence ($\alpha = 0°$). At the resonance frequency $f_{\mathrm{res}} = 2.9$ THz, $T = 4.5\%$, $R = 1.5\%$, and $A = 94.0\%$.

$\alpha = 20°$, 40°, and 60° for both TE- and TM-waves. The reflectance shows an asymmetrical frequency dependence, which differs between TE- and TM-waves, but the spectra clearly demonstrate that the absorber is effective for both TE- and TM-polarizations. Furthermore, whereas the device is strongly frequency selective for the transmittance, the array demonstrates effective anti-reflection properties in a wide frequency range. The decrease in absorptance with increasing angle of incidence is noticeable, but around the resonance frequency, the absorptance is almost constant for angles of incidence up to ~40°. Absorptance spectra calculated for $\alpha = 80°$ have peak resonant values $A_{\mathrm{TE}} = 0.48$ and $A_{\mathrm{TM}} = 0.35$.

The relative spectral width, $\Delta f/f_{\mathrm{res}}$, with Δf the spectral width at half maximum, of the absorptance spectra is presented in Table 1.

Figure 6 illustrates the absorber's mechanism of operation at the resonant frequency. At resonance, a normally

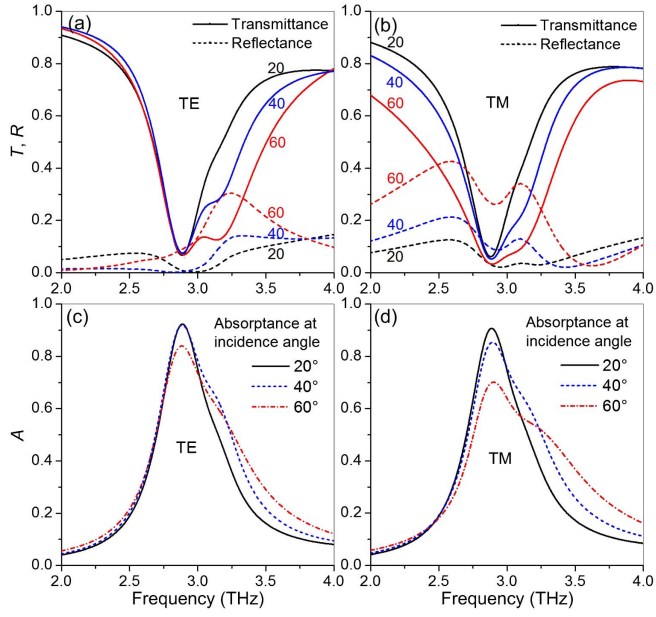

Fig. 5. Transmittance, reflectance, and absorptance spectra for TE polarization (a, c), and for TM polarization (b, d). Three angles of incidence are considered: 20°, 40°, and 60°.

Table 1. Relative Spectral Width of Absorptance Spectra

Incidence Angle	0°	20°	40°	60°	80°
TE	0.14	0.17	0.20	0.23	0.46
TM	0.14	0.17	0.21	0.29	0.48

incident electromagnetic wave generates a strong electric current in the omega particles. The current is indicated by small arrows with thickness and density proportional to the current density. Figures 6(a) and 6(b) represent two cases, with an incident radiation phase difference of 90°. In the case of Fig. 6(a), the four in-plane omegas of each unit cell are excited, whereas in Fig. 6(b), the four out-of-plane omegas are excited. The induced electric (**p**) and magnetic (**m**) moments are equal in magnitude, due to the optimal geometry of the omega particles for the resonant frequency. However, the vectors in the differently arranged omegas of each unit cell have different directions. In the case of Fig. 6(a), the magnetic responses cancel each other, and the same happens with the electric responses in Fig. 6(b). The resulting pure electric and magnetic responses (bianisotropy compensation), oscillating with a phase difference of 90°, cause strongly scattered electromagnetic waves. Their phase is opposite to that of the transmitted waves [14], and therefore at resonance, transmission is virtually completely blocked. The energy of the wave is dissipated and transferred into heat. Theoretical details of the effect of near-perfect absorptance are shown in [10] for the exemplary case of helical inclusions [16,17] with compensated chirality; however, the general theoretical model is also valid for other bianisotropic particles.

All omega particles of Figs. 1, 3 and 6 are separate, that is, they do not touch each other. It is of interest to consider the array's action when the omegas make contact. Figure 7 demonstrates the reflectance, transmittance, and absorptance of the omega metamaterial with locked loops. In this regime, the pixels are open, and because the electromagnetic responses in the unit cell are weak [see the inset in Fig. 7], the resulting transmittance is high at

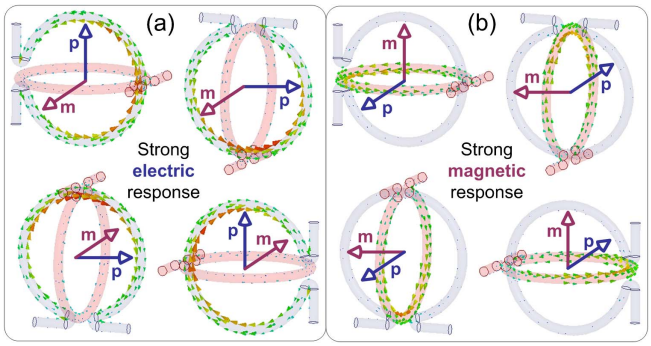

Fig. 6. Electric currents induced in the omega particles of a unit cell by means of a normally incident wave at $f_{res} = 2.9$ THz. The incident waves in (a) and (b) have a phase difference $\pi/2$. In (a) locally induced magnetic responses cancel each other, but in (b) locally induced electric responses cancel each other. Consequently, in a unit cell pure electric and pure magnetic responses oscillate with phase difference $\pi/2$, causing destructive interference of transmitted waves.

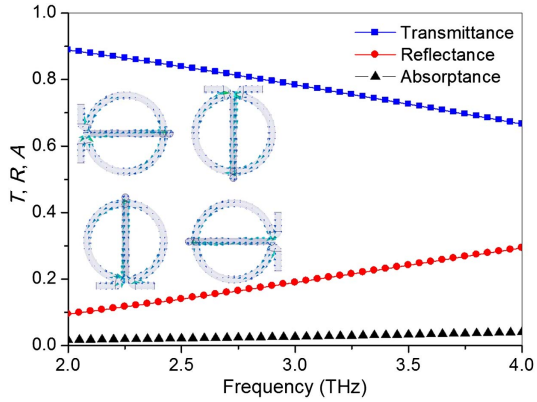

Fig. 7. Transmittance, reflectance, and absorptance versus frequency for radiation normally incident ($\alpha = 0°$) at an array of locked omega resonators. Inset: electric currents in the locked omega particles.

all frequencies. Closing the omegas can occur through shrinking the omega's diameter, but alternatively, the gap can also be closed by twisting the paired particles with regard to each other by ~40°. In the latter case, the spectra are almost identical to those of Fig. 7.

As the gap is small, it can be closed by embedding into the gap a material with externally controllable conductivity that can be activated optically, magnetically, or electronically by applying external light, magnetic field, or voltage. Also thermal expansion due to heating of the omegas could be used to close the gap and consequently to increasing the transmittance.

The proposed metamaterial can be utilized in THz vision applications by making it an active transmitter with the possibility of independently switching pixels that change their state from opaque to transparent and vice versa.

The array of omega particles can be produced by lithographic methods, fixed in a transparent medium such as Teflon. In the modeling, we assumed a medium fully transparent for THz radiation, but with for instance a 0.1-mm-thick Teflon substrate, the transmittance for frequencies around 3 THz is $T \sim 90\%$. For the material of the omega particles, a metal with high ohmic loss has to be used to get strong dissipation of energy. In our calculations, we used titanium (electric conductivity $1.82 \cdot 10^6$ S/m), because it is durable and has a low thermal expansion coefficient. However, the maximum absorptance can be slightly increased to 97% when using a platinum-ruthenium alloy. Obviously the spectral characteristics will depend on the substrate and particle material and thus will require adjusted geometrical parameters for the omega particle array.

The omega array presented here demonstrates its potential for a frequency-selective, near-perfect absorber at THz frequencies for radiation incident from either side. The array can be fabricated by laser lithography methods with subsequent metallization or ion beam-selective etching. It can be produced in a flexible substrate that facilitates the development of roll-up absorbers and displays. As for other applications, it is interesting to note that the absorber may be loaded with diodes so to collect impinging radiation and convert it into electricity [18].

Moreover, the unit cell (pixel) can be made switchable and implemented in single-pixel THz imaging techniques. In the THz frequency regime, the proposed metamaterial has substantial potential for being used for spatial light modulators, sensors, and bolometers [10,19].

References

1. N. Landy, S. Sajuyigbe, J. Mock, D. Smith, and W. Padilla, Phys. Rev. Lett. **100**, 207402 (2008).
2. J. Grant, Y. Ma, S. Saha, A. Khalid, and D. R. S. Cumming, Opt. Lett. **36**, 3476 (2011).
3. H. Tao, C. Bingham, A. Strikwerda, D. Pilon, D. Shrekenhamer, N. Landy, K. Fan, X. Zhang, W. Padilla, and R. Averitt, Phys. Rev. B **78**, 241103 (2008).
4. R. Yahiaoui, J. P. Guillet, F. de Miollis, and P. Mounaix, Opt. Lett. **38**, 4988 (2013).
5. P. Bouchon, C. Koechlin, F. Pardo, R. Haïdar, and J. Pelouard, Opt. Lett. **37**, 1038 (2012).
6. S. Chen, H. Cheng, H. Yang, J. Li, X. Duan, C. Gu, and J. Tian, Appl. Phys. Lett. **99**, 253104 (2011).
7. M. K. Hedayati, M. Javaherirahim, B. Mozooni, R. Abdelaziz, A. Tavassolizadeh, V. S. K. Chakravadhanula, V. Zaporojtchenko, T. Strunkus, F. Faupel, and M. Elbahri, Adv. Mater. **23**, 5410 (2011).
8. T. Cao, C. Wei, R. E. Simpson, L. Zhang, and M. J. Cryan, Sci. Rep. **4**, 3955 (2014).
9. I. A. Faniayeu, V. S. Asadchy, T. A. Dziarzhauskaya, I. V. Semchenko, and S. A. Khakhomov, "A single-layer meta-atom absorber," in *Metamaterials 2014* (IEEE, 2014), pp. 112–114.
10. V. S. Asadchy, I. A. Faniayeu, Y. Ra'di, S. A. Khakhomov, I. V. Semchenko, and S. A. Tretyakov, "Broadband reflectionless metasheets: frequency-selective transmission and perfect absorption," http://arxiv.org/abs/1502.06916v1 (2015).
11. A. Serdyukov, I. Semchenko, S. Tretyakov, and A. Sihvola, *Electromagnetics of Bi-Anisotropic Materials: Theory and Applications* (Gordon and Breach, 2001).
12. I. V. Semchenko, S. A. Khakhomov, M. A. Podalov, and S. A. Tretyakov, J. Commun. Technol. Electron. **52**, 1002 (2007).
13. A. Balmakou, I. Semchenko, and M. Nagatsu, Opt. Lett. **38**, 3499 (2013).
14. B. M. Yavorsky, A. A. Detlaf, and N. Weinstein, *Handbook of Physics*, 4th ed. (Central Books, 1973), p. 965.
15. I. V. Semchenko, S. A. Khakhomov, and A. L. Samofalov, Eur. Phys. J. Appl. Phys. **49**, 33002 (2010).
16. A. Balmakou, I. Semchenko, and M. Nagatsu, Appl. Phys. Express **6**, 072601 (2013).
17. A. Balmakou, I. Semchenko, and M. Nagatsu, Progr. Electromagn. Res. M **31**, 231 (2013).
18. A. M. Hawkes, A. R. Katko, and S. A. Cummer, Appl. Phys. Lett. **103**, 163901 (2013).
19. C. M. Watts, D. Shrekenhamer, J. Montoya, G. Lipworth, J. Hunt, T. Sleasman, S. Krishna, D. R. Smith, and W. J. Padilla, Nat. Photonics **139**, 1 (2014).